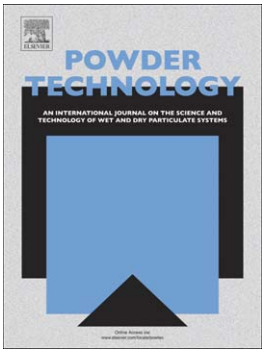

Contamination during the high-energy milling of atomized copper powder and its effects on spark plasma sintering

G. Cipolloni, M. Pellizzari, A. Molinari, M. Hebda, M. Zadra

PII: S0032-5910(15)00090-X
DOI: doi: 10.1016/j.powtec.2015.01.063
Reference: PTEC 10778

To appear in: *Powder Technology*

Received date: 9 October 2014
Revised date: 19 January 2015
Accepted date: 24 January 2015

Please cite this article as: G. Cipolloni, M. Pellizzari, A. Molinari, M. Hebda, M. Zadra, Contamination during the high-energy milling of atomized copper powder and its effects on spark plasma sintering, *Powder Technology* (2015), doi: 10.1016/j.powtec.2015.01.063

Contamination during the high-energy milling of atomized copper powder and its effects on spark plasma sintering

G. Cipolloni, M. Pellizzari, A. Molinari, M. Hebda, M. Zadra

Corresponding author

Dr. Giulia Cipolloni

Department of Industrial Engineering, University of Trento

Via Sommarive 9, 38123 Trento, Italy

Phone: +390461282402

Email: g.cipolloni@unitn.it

Abstract

Mechanical milling is a suitable technique to enhance various properties of copper by the severe plastic deformation involved during the process. Contamination from milling media is one of the major problems of mechanical alloying. In this study, the behaviour of copper powder during mechanical milling was investigated in order to minimize iron and chromium contaminations. Hence, three different parameters have been studied to highlight the high influence of ball milling parameters on the final products. The parameters included the type of process control agent (none, toluene or stearic acid), the ball-to-powder weight ratio (33:1 or 10:1) and finally, a change in the milling cycle (interrupted or continuous) in an interactive procedure according to the experimental results. As a result, the best morphology and contamination level combination was observed in powder milled with stearic acid; it was 10:1 for the ball to powder ratio when using a continuous milling cycle. Once the best milling conditions were determined, the resulting samples were exposed to spark plasma sintering (SPS). The sintering parameters were selected based on a previous thermal gravimetrical measurement of the milled powders to avoid residual porosity. The final density of all of the samples is very good, 99%, confirming an effective densification process and sintering activated by severely strain-hardened and nanostructured particles.

Keywords

Atomized copper powder; mechanical milling parameters; contamination; spark plasma sintering

1 Introduction

Mechanical alloying is a solid-state powder processing technique involving repeated welding, fracturing and re-welding of powder particles in a high-energy ball mill [1]. In recent years, ball milling has attracted considerable interest due to the wide range of materials exhibiting good properties that can be fabricating using this process, especially in the production of metal matrix composites [2-5]. A major issue with this process is the contaminations that arise from the milling medium and the atmosphere [6-8]. Copper contaminations could negatively affect the electrical and thermal conductivity by acting as a barrier to the electrical and thermal flow [6-9]. Even if milling in a

highly pure inert atmosphere or a vacuum avoids contaminations from the atmosphere [1], contaminations resulting from the milling medium are unavoidable. Contaminates depend on the nature of the raw materials [10-12] and the milling conditions. Here, the importance of optimizing the milling parameters are discussed [13].

It was found that metallic powder can easily form a thin coating on the surface of grinding balls and the inner walls of the containers, especially in the case of ductile powders [14]. This coating may decrease contamination by preventing the milling medium from contacting the milled powders [15]. Creating a ductile coating on the milling medium surface prior to the addition of the hard particles could be a good solution in the production of metal matrix composites. Process parameters such as the use of a process control agent, the ball-to-powder weight (charge) ratio and the milling time play an important role in the nature and kinetics of the formation of the protective layer [1].

The use of a process control agent (PCA) overcomes the contamination of the final powder caused by the repeated collision that the powders sustain against the grinding bodies [6]. Moreover, in the absence of a process control agent, there is a predominance of welding events over the fractures, which resulted in the production of hollow spherical particles up to millimetres in diameter [9; 16]. Therefore, it is also important to inhibit welding events to produce a fine powder, and it is generally necessary to use a specific process control agent or to cool the vial by an interrupted milling cycle [1]. The choice of a PCA depends on the nature of the powder being milled and the purity of the final products [17-19].

Another important variable in the milling process is the ball-to-powder mass ratio (BPR). At a high BPR, the number of collisions per unit time increases; consequently, more energy is transferred to the powder particles. Mechanical alloying occurs faster [20-21], but at the same time, the abrasion of the milling medium increases at a high BPR. Moreover, a high BPR decreases the milling time while increasing the internal temperature, which may promote unwanted reactions [22]. An interrupted cycle is, therefore, preferable in order to cool the vial, even if it increases the milling time.

Mechanical alloying refines the structure of the powders, leading to ultrafine and nanosized grain size. Such features are required to be maintained during sintering to obtain materials with high mechanical resistance. Spark plasma sintering (SPS) is perhaps the most suitable technology for this purpose. The simultaneous application of pressure and pulsed continuous current, the fast heating rate and the short sintering time make SPS an excellent technology by which highly dense, bulk, ultrafine and nanostructured materials can be obtained [23-28].

The objective of this study was to systematically investigate how milling conditions affect contamination in the milled powder. Moreover, the decomposition of PCA has been analysed to determine the parameter of the SPS cycle to minimize the residual porosity. Meanwhile, the morphology of the milled powders, the microstructure, the density and the hardness of the sintered products were also investigated.

2 Materials and Method

A water atomized copper powder (99.55%) was used. Mechanical milling was conducted in a Fritsch Pulverisette 6 planetary mono mill at 400 rpm in a vacuum (0.13 mbar). A 0.5%wt PCA of either toluene or stearic acid was added. Vials and spheres in 100Cr6 (63 HRC) with diameters of 10 mm were used to obtain ball-to-powder ratios of 33:1 and 10:1 (in mass). Two different milling strategies were investigated: interrupted operation at 2 minutes on and 9 minutes off for an effective total milling time of 20 (time I) and 200 minutes (time II); continuous cycles for the same effective time period. In Table 1, all of the different milling conditions are reported. The powder morphology was characterized by quantitative image analysis of the metallurgical cross sections of the particles. To obtain statistical support, at least 10 optical micrographs for each sample were considered. Two distinct parameters were analysed, namely, the particle cross sectional area and the aspect ratio, i.e., the ratio between the maximum and minimum length of each particle. The first parameter is representative of the particle size, while the second is representative of the particle morphology. The iron and chromium contamination of the powder was measured by an inductively coupled plasma mass spectrometry (ICP), while oxygen and carbon content were measured by combustion analysis (LECO). The same analyses were carried out on the sintered samples. Thermo-

gravimetrical analyses of the milled powders were carried out in an argon atmosphere at a temperature of up to 1060°C and with a heating rate of 20°C/min; these analyses were combined with quadrupole mass spectrometry STA409CD (Netzsch). The powders were sintered in a DR.SINTER® SPS1050 (Sumitomo Coal & Mining, now SPS Syntex, Inc.) apparatus with graphite punches and dies. All samples had cylindrical geometry with a height of 5 mm and a diameter of 20 mm. SPS was performed at a nominal temperature (measured with a thermocouple inserted into a blind hole in the die wall) of 950°C, with a uniaxial pressure of 30 MPa applied at 700°C. The heating rate was 100°C/min up to 900°C and 50°C/min up to the sintering temperature. The maximum temperature and pressure were held for 1 and 3 minutes, respectively, before allowing the furnace to cool to room temperature. The density of the SPS-processed pellets was measured according to Archimedes' principle, considering the theoretical densities of pure Cu as 8.96 gm/cm^3. Vickers micro-hardness of sintered samples was measured using a Vickers Paar MHT-4 micro-indenter by applying a load of 0.5 N at a rate of 0.05 N/s and with a dwell time of 10 s. Scanning electron microscopy (SEM) was performed with a Philips XL30 apparatus for the observation of the powder and of the fracture surface of the sintered specimens. The metallographic cross section of the sintered samples was obtained by precision micro-cutting with a diamond blade. Standard metallographic preparation was also accomplished, including grinding with SiC papers up to 4000 grit, final polishing with 3-µm and 1-µm diamond pastes, and chemical etching with 120 mL of distilled water, 30 mL of hydrochloric acid and 10 g of iron chloride [29]. The microstructure was also evaluated using an optical microscope.

3 Results and discussion

3.1 Powder characterization

Figure 1 shows a SEM micrograph of the atomized Cu powder and a metallographic cross-section obtained using the optical microscope. Copper is characterized by the irregular morphology typical of the water atomization process and by particle sizes smaller than 75 microns. Figure 2 shows the SEM micrographs of the milled powder. The particle size increases after mechanical milling because copper is very ductile; this favours the predominance of welding events over fracturing actions. The particle size

increases with milling time, and the morphology changes towards a flake shape, especially without any PCA use. The benefit of using a PCA is evident because it impedes the clean metal-to-metal contact necessary for cold welding and leads to the dispersion of aggregates. In turn, milling efficiency is improved, especially in the case of toluene (Fig. 2). Additionally, the image analysis results confirm the effectiveness of PCA in reducing the particle size (Fig. 3). When using toluene after 200 minutes, the particles are smaller (Fig. 2 cI-II), more uniform and more equiaxed than after 20 minutes (Fig. 3b). Instead, when using stearic acid, the particles show intense flake morphology and a size decrease after 20 minutes (Fig. 3a). Meanwhile, increasing the milling time allows the particles to become larger and thicker because welding prevails on fracturing and the aspect ratio tends to decrease due to the achievement of a more equiaxed morphology (Fig. 3b). Nevertheless, particle size is smaller than in the case of dry milling (Fig. 2 dII-bII), and the improved morphology using toluene and stearic acid is highlighted by the lower aspect ratio after 200 minutes of milling (Fig. 3b). From the morphological point of view, toluene is the best process control agent due to its high wettability, which allows intense fragmentation of the particles for a longer milling time and results in powders that are fine and uniformly sized, even after 200 minutes.

PCA has two effects on ball milling. One effect is the decrease of the viscosity of the slurry of the powder mixture which enhances the grinding rate [19]. The other effect is the reduction of wear on the hard and brittle balls and, in turn, of the contamination of the milled powder. The second benefit is attested to by the ICP test, as shown by the results of the chemical analysis of the milled powder reported in Figure 4, relevant to the interrupted cycle with a ball-to-powder ratio of 33:1.

The content of Fe end Cr impurities in the milled powder increases when the milling time increases. The lowest amount of contamination is observed when using stearic acid; for example, with reference to dry milling, the iron contamination decreases from 0.25% and 0.35% after 20 and 200 minutes, respectively, to 0.04% and 0.06%. Stearic acid aids in the creation of a protective layer all over the balls and the vial. This avoids the excessive abrasion of the milling medium caused by the high impact events. This result is very important for those applications using copper that have a relationship with

its outstanding electric and thermal properties [6; 9]. Therefore, in spite of the larger particle size obtained with the stearic acid with respect to toluene, the former PCA was selected for the next step in this work.

The influence of the BPR has also been studied, and Figure 5 shows the powder morphology after milling with a BPR of 10:1.

In Figure 5, the morphology of the powder changes drastically towards a lamellar morphology, especially after 200 minutes, compared to Figures 3dI-II. After 20 minutes of milling, the powder presents a flaky morphology, but the particles are thicker than after being milled for 200 minutes. With a large BPR, mechanical milling has the tendency to produce larger aggregates with an increased milling time due to the higher amount of impact events and the increase in the internal temperature [15; 17]. Instead, with a small BPR, fracturing predominates the welding, especially for long milling times (Fig. 5e-II). Less heat input due to the use of a lower BPR does not require cooling pauses, and this allows for the replacement of the interrupted cycle with the continuous one. The final product must guarantee the requested properties. The morphology of the powder from the continuous cycle is shown in Figure 6. It is clear that the particle dimensions are not increased with respect to the interrupted cycle, and no aggregates are present. Especially for a longer milling time, the powder still shows a lamellar morphology but a smaller size than in the case of an interrupted cycle.

As far as contamination is concerned, the choice of a lower BPR and a continuous cycle seems to be the right one, as shown in Table 2. Chromium contamination is not reported because it was approximately zero compared to the previous results. It is evident how decreasing the ball-to-powder ratio from 33:1 to 10:1 significantly decreases the amount of Fe contamination.

According to the present results, the continuously milled copper powder with 0.5wt% stearic acid, a BPR of 10:1 and a continuous cycle have been selected for the next sintering process.

The presence of stearic acid may result in C and O contamination that may affect the behaviour of the powder during sintering. In Table 3, the amount of oxygen and carbon after milling are reported.

The oxygen and carbon contents increase significantly. The higher level of oxygen after 200 minutes of milling is associated to the oxidation of the powder occurring during ball milling. In Figure 7, the results of the TGA are displayed for atomized copper and for copper milled for 20 and 200 minutes with stearic acid. The diagram of the atomized copper shows a continuous mass loss until 500°C is reached. Conversely, the milled powder shows a higher mass loss with an increase in milling time, indicating that three different events occurred at different temperatures, i.e., 150°C, 300°C and 450°C. According to quadrupole mass spectrometry, these events could be correlated with different gas emissions, as follows:

(a) 100°C - 1000°C, continuous water evaporation;

(b) 300°C, water evaporation and production of CO and especially CO_2;

(c) 450°C, H_2 production.

In the case of atomized copper, only water evaporation occurs as long as a continuous weight loss has been detected by the TGA up to 500°C and no PCA is present. In the case of milled powder, the slope of the TGA curve also depends on the mass of the evaporated element. For this reason, the second segment (300°C) presents a higher slope due to the higher mass of CO and CO_2 than that of the H_2O and H_2 molecules. The powder milled for 20 minutes exhibits intermediate behaviour because the milling time is not sufficient to ensure a complete homogenization of the powder. In this way, the test is affected by the powder batch selected. In fact, the CO_2 peak at 300 °C is less evident compared to the case of the powder milled for 200 minutes; this is due to the incomplete dispersion of stearic acid in the powder. From these results, in order to allow proper decomposition of the stearic acid and to avoid any gas entrapment favouring porosity, the pressure during SPS will be applied only when the temperature reaches 700°C.

3.2 Spark Plasma Sintering

Figure 8 displays the load and vacuum curves during the SPS cycle for the atomized and mechanically milled powders. First, there is an excellent correspondence between the vacuum trend (Fig. 8) and the

ion current recorded by quadrupole mass spectroscopy (Figs.7a-b-c). This agreement highlights the reliability of the vacuum level as a useful measurement for the analysis of gas emissions. Finally, the residual oxygen and carbon measurements after sintering were completed, and the results are reported in Table 4.

It is clear how the amounts of oxygen and carbon are drastically decreased during sintering. An important result is that the amount of oxygen and carbon residual is halved after sintering, confirming the release of some gases, especially CO and CO_2. The final oxygen content (0.21 and 0.37%) can be attributed to the presence of magnesium in the starting powder, which easily oxidizes at high temperature and promotes the formation of stable magnesium oxide [30]. Figure 9 displays the lower punch displacement curves for the as atomized powder (dashed line) and the milled powder after 20 minutes (solid line) and after 200 minutes (bold line), respectively. Notably, the sharp displacement at 700°C is due to the pressure application at this temperature.

The displacement curve is widely accepted as a densification measure as a function of the sintering temperature. However, in spite of the high and similar density after sintering (99%) (Table 5), the final displacement of the atomized powder (7 mm) is much higher than that of the milled powders (~4 mm). The reason for this apparently anomalous behaviour is found in the apparent density of the two powders. The milled powder is characterized by a flaky morphology and smaller particle size (Fig. 6 fI-II) than the atomized copper (Fig. 1). This promotes a high packing factor associated with a higher apparent density [31-34]. It is also believed that the presence of residual stearic acid in the milled powder aids the particle rearrangement by its lubricating action. Finally, it is clear that this powder can reach the same density with a shorter punch stroke and, therefore, a lower final displacement. Figure 9 shows that, in all cases, the displacement reaches a plateau, confirming the complete densification.

The densification behaviour can be studied considering two parts of the displacement curves, namely, before and after the application of pressure at 700°C. For comparison purposes with previous results [32], the first displacement derivative, which represents the densification rate, is reported as a function of the sintering temperature (Fig. 10).

Under a load-free densification regime, the atomized powder starts to densify at 400°C (dashed line). The punch displacement corresponds to a first peak at approximately 600°C (Fig. 10), which could be correlated with the previously determined bulk deformation values of Cu powders [32]. According to [32-37], atomized Cu is not yet sintered at such a low temperature because the mass transport phenomena responsible for the neck formation and growth mainly occurs between 650°C and 900°C. When the pressure is applied at 700°C, the atomized powder shows a severe displacement increase because the deformation extends to the core of the particles, improving densification. The high compressibility of the atomized powder promotes a full densification associated with a higher displacement rate. In the case of the atomized powder, the densification process is successfully completed at 900°C when the displacement rate drops to zero.

Powders milled for 20 minutes show an intermediate behaviour between those of the atomized and long-time milled powders because the powders had not been uniformly milled. A first peak is evident at 400°C, followed by a second peak at 600°C; these could be correlated to the bulk deformation. When the load is applied, a third peak is evident at 750°C, which is less intense than in the case of the atomized powder because milled powders oppose a greater deformation resistance due to the strain hardening caused by milling.

The displacement curves of the powders milled for 200 minutes (Fig. 9) show a gradual and progressive densification from the start of the process, i.e., still at very low temperature (>100°C). This behaviour highlights an activation of the process induced by the different morphology and the higher sinterability of the milled powders. First, the electrical resistance $R= \rho h/S$ *(ρ=el. resistivity of Cu, h=sample thickness, S=contact area between particles)* decreases with the extension of the contact area [36]. This is ultimately reflected in an enhanced local deformation of the flake particles. Moreover, powders subjected to extensive mechanical milling undergo severe strain hardening and strong reduction of the crystallite size, allowing nanostructuring and an increased powder sinterability. For both these reasons, the bulk densification of the milled powder is also promoted by sintering. This supports the higher densification of milled powders for 200 minutes, as demonstrated by the higher displacement during the first regime (Fig.

9). Furthermore, the displacement rate of milled powder at 600°C is lower than the displacement rate of atomized copper because the densification begins earlier and occurs more gradually than in atomized powder.

Under pressure, the displacement of milled powders is lower because most of the densification and sintering occurred in the previous step. The lower densification, also evidenced by the lower intensity of the displacement rate peak, can be attributed at least in part to the heavy plastic deformation induced by milling. In the case of milled powder, the densification the process is successfully completed at 850°C (Fig. 10). To better investigate the effectiveness of sintering, specimens were broken to observe the fracture surfaces, which are reported in Figure 11.

The fully dimpled surfaces prove the ductile nature of the fractures and the effective consolidation of the material, especially for atomized powder. In the milled sample, the morphology of the dimples and the elongated perpendicularly to the deformation direction are clearly affected by the heavy straining of particles during mechanical milling. Additionally, a microstructural analysis has been completed, and the micrographs are reported in Figure 12.

The sample sintered from the atomized powder (Fig. 12a) shows a uniform microstructure; however, the sample from the milled powders (Fig. 12b-c) shows an intrinsic anisotropy due to its flaky morphology, especially for powder milled for 200 minutes.

As stated previously, the relative density of the samples from the milled powder is equal to the density from the atomized powder (99%), in spite of the higher hardness of the first powders (Table 5). This is supported by hardness measurements, which highlight a greater hardness for the milled samples even after sintering. It can be concluded that high temperature exposure, even if for a short time, does not completely remove the strain hardening effects induced by milling. Mechanical milling induces a hardness increase, and the promotion of hardening by longer milling times is confirmed by the higher hardness values after 200 minutes of milling. The measurements have been carried out on the surface, parallel to the direction of the force applied during SPS, even on the perpendicular surface. In this way, the intrinsic anisotropy is analysed for all of the powders. Even the starting powder shows a

difference between the two directions, so the anisotropy is related both to the morphology of the milled powder and to the sintering process. When the hardness load measurement is taken parallel to the compaction direction, the hardness is higher than in the opposite case.

4 Conclusions

In the first section of this study, the effect of different milling conditions was studied based on the use of stearic acid as a process control agent aiding the creation of a protective internal layer over the milling medium to overcome the contaminations problem. The use of a ball-to-powder ratio of 10:1 instead of 33:1 considerably reduces the Fe and Cr contamination; moreover, it reduces the involved high impact energy and its associated increase in temperature. The lower heat input due to the lower BPR allowed cooling pauses to be avoided during milling, so the interrupted cycle was replaced with a continuous cycle. The absence of a pause to cool the temperature during milling did not negatively affect the final particle size or the contamination level. The TGA analysis allowed the best sintering cycle to be determined in order to limit the residual porosity of the final product. The SPS cycle could be properly designed with pressure (30 MPa) application at 700°C for 3 minutes and sintering at 950°C for 1 minute. In the second study section, densification and sintering was investigated. Densification is promoted by the correct evaporation of the residual gases of the process control agent during sintering. The final density of all of the samples is very good at 99%, confirming an effective densification process and sintering activated by severely strain-hardened and nanostructured particles. Moreover, the hardness increases with milling time, showing an intrinsic anisotropy due to both the high flaking level and the direction of the compaction pressure.

Acknowledgements

The authors gratefully acknowledge Pometon Powder Company for the supply of copper powder and for the ICP-LECO analysis. This research was supported by Professor J. Kazior at the Institute of Materials Engineering, Cracow University of Technology.

References

[1] C.Suryanarayana, Mechanical alloying and milling, Progress in Materials Science 46 (2001) 1-184.

[2] F.Akhtara, S.J.Askaria, K.A.Shaha, X.Dua, S.Guoa, Microstructure, mechanical properties, electrical conductivity and wear behavior of high volume TiC reinforced Cu-matrix composites, Materials Characterization 60 (2009) 327-336.

[3] K.Dash, B.C.Ray, D.Chaira, Synthesis and characterization of copper–alumina metal matrix composite by conventional and spark plasma sintering, Journal of Alloys and Compounds 516 (2012) 78-84.

[4] B.D.Longa, R.Othmana, M.Umemotob, H.Zuhailawatia, Spark plasma sintering of mechanically alloyed in situ copper–niobium carbide composite, Journal of Alloys and Compounds 505 (2010) 510-515.

[5] H.Wang, W.Wua, S.Sun, X.Bian, G.Tu, Characterization of the structure of TiB2-TiC nanocomposite powders fabricated by high-energy ball milling, Ceramics International 37 (2011) 2689-2693.

[6] M.Lopez, D.Corredor, C.Camurri, V.Vergara, J.Jime´nez, Performance and characterization of dispersion strengthened Cu–TiB2 composite for electrical use, Materials Characterization 55 (2005) 252-262.

[7] X.T.Luo, C.J.Li, G.J.Yang, Correlations between milling conditions and iron contamination, microstructure and hardness of mechanically alloyed cubic BN particle reinforced NiCrAl matrix composite powders, Journal of Alloys and Compounds 548 (2013) 180–187.

[8] A.Sato, J.Kano, F.Saito, Analysis of abrasion mechanism of grinding media in a planetary mill with DEM simulation, Advanced Powder Technology 21 (2010) 212–216.

[9] B.D.Longa, H.Zuhailawatia, M.Umemotob, Y.Todakab, R.Othmana, Effect of ethanol on the formation and properties of a Cu–NbC composite, Journal of Alloys and Compounds 503 (2010) 228-232.

[10] J.S.Benjamin, T.E.Volin, The mechanism of MA, Metallurgical Transactions (1974) 5 1929-34.

[11] P.Y.Lee, C.C.Koch, Journal of Material Science (1988) 23 2837-45.

[12] R.M.Davis, C.C.Koch, Scripta Metallurgia (1987) 21 305-10.

[13] F.L.Zhang, M.Zhu, C.Y.Wang, Parameters optimization in the planetary ball milling of nanostructured tungsten carbide/cobalt powder, International Journal of Refractory Metals and Hard Materials 26 4 (2008) 329-333.

[14] M.S.El-Eskandarany, K.Aoki, K.Suzuki, Rod milling for solid-state formation of $Al_{30}Ta_{70}$ amorphous alloy powder, Journal of Less-Common Metals 167 1 (1990) 113–118.

[15] L.Hao, Y.Lu, H.Asanum, J.Guo, The influence of the processing parameters on the formation of iron thin films on alumina balls by mechanical coating technique, Journal of Materials. Processing Technology 212 (2012) 1169-1176.

[16] A.M.Harris, G.B.Schaffer, N.W.Page, The morphological evolution of hollows shells during the mechanical milling of ductile metals, Scripta Materialia 34 (1996) 67-73.

[17] Y.F.Zhang, L.Lu, S.M.Yap, Prediction of the amount of PCA for mechanical milling, Journal of Materials Processing Technology 89-90 (1999) 260-265.

[18] C.P.Samal, J.S.Parihar, D.Chaira, The effect of milling and sintering techniques on mechanical properties of Cu–graphite metal matrix composite prepared by powder metallurgy route, Journal of Alloys and Compounds 569 (2013) 95-101.

[19] K.Suzuki, Effects of fluid on vibration ball milling grinding, Journal of Chemical Engineering Jpn 19 (1986) 191-195.

[20] Q.Zeng, Y.F.Xiao, S.Z.Dong, X.B.Liu, B.Q.Qiu, Z.Y.Zhang, R.Wang, Influence of milling conditions on magnetic properties of $Nd(Fe,Mo)_{12}Nx$ compounds, Journal of Magnetism and Magnetic Materials 192 2 (1999) 321-324.

[21] S.Xi, J.Zhou, X.Wang, D.Zhang, Journal of Materials Science Letters (1996) 15 634-9.

[22] M.Khitouni, R.Daly, M. Mhadhbi, A.Kolsi, Structural evolution in nanocrystalline Cu obtained by high-energy mechanical milling: Phases formation of copper oxides, Journal of Alloys and Compounds 475 (2009) 581-586.

[23] R.Orrù, R.Licheri, A.M.Locci, A.Cincotti, G.Cao, Consolidation/synthesis of materials by electric current activated/assisted sintering, Materials Science and Engineering. R. 63 (2009) 127-287.

[24] M.Omori, Sintering, consolidation, reaction and crystal growth by the spark plasma system (SPS), Materials Science and Engineering A 287 (2000) 183-188.

[25] M.Tokita, Mechanism of Spark Plasma Sintering, Journal of the Society of Powder Technology Japan 30 (1993)790-804.

[26] V.Mamedov, Spark plasma sintering as advanced PM sintering method, Powder Metallurgy 45 (2002) 322-328.

[27] Z.Zhaohui, W.Fuchi, W.Lin, L.Shukui, S.Osamu, Sintering mechanism of large-scale ultrafine-grained copper prepared by SPS method, Materials Letters 62 (2008) 3987-3990.

[28] Z.H. Zhang, F.C.Wang, L.Wang, S.K.Li, Ultrafine-grained copper prepared by spark plasma sintering process, Materials Science and Engineering A 476 (2008) 201-205.

[29] G.Petzow, Metallographic Etching, (1999)

[30] C.Menapace, M.Zadra, A.Molinari, C.Messner, P.Costa, Study of microstructural transformations and dimensional variations during liquid phase sintering of 10% tin bronzes produced with different copper powders, Powder Metallurgy 45 (1) (2002) 67.

[31] K.Gan, M.Gu, The compressibility of Cu/SiCp powder prepared by high-energy ball milling, Journal of Materials Processing Technology 199 (2008) 173-177.

[32] S.Diouf, A.Molinari, Densification mechanism in spark plasma sintering: effect of particle size and pressure, Powder Technology 221 (2012) 220-227.

[33] S.Diouf, C.Menapace, A.Molinari, Study of effect of particle size on densification of copper during spark plasma sintering, Powder Metallurgy 55 (3) (2012) 228-234.

[34] A.Fedrizzi, M.Pellizzari, M.Zadra, Influence of particle size ratio on densification behaviour of AISI H13/AISI M3:2 powder mixture, Powder Technology 228 (2012) 435-442.

[35] X.Song, X.Liu, J.Zhang, Neck formation and self-adjusting mechanism of neck growth of conducting powders in spark plasma sintering, Journal of American Ceramic Society 89 (2006) 494-500.

[36] S. Diouf, Production of a nanostructured copper by Spark Plasma Sintering, Doctoral Thesis, (2013).

[37] M.Pellizzari, A.Fedrizzi, M.Zadra, Spark Plasma co-Sintering of hot work and high speed steel powders for fabrication of a novel tool steel with composite microstructure, Powder Technology, 214 (2011) 292-299.

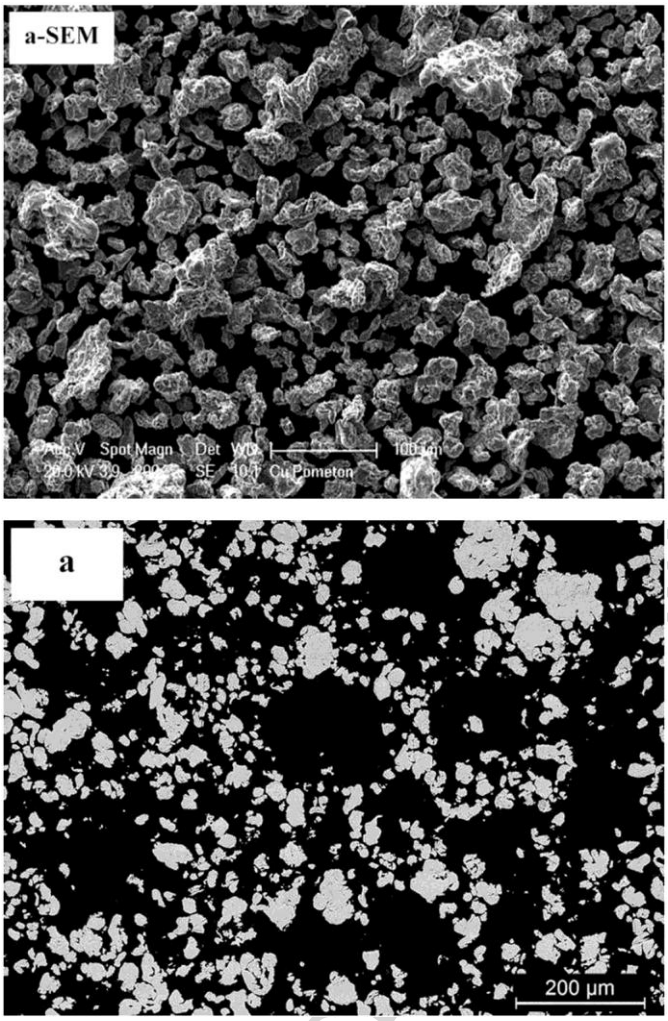

Fig 1

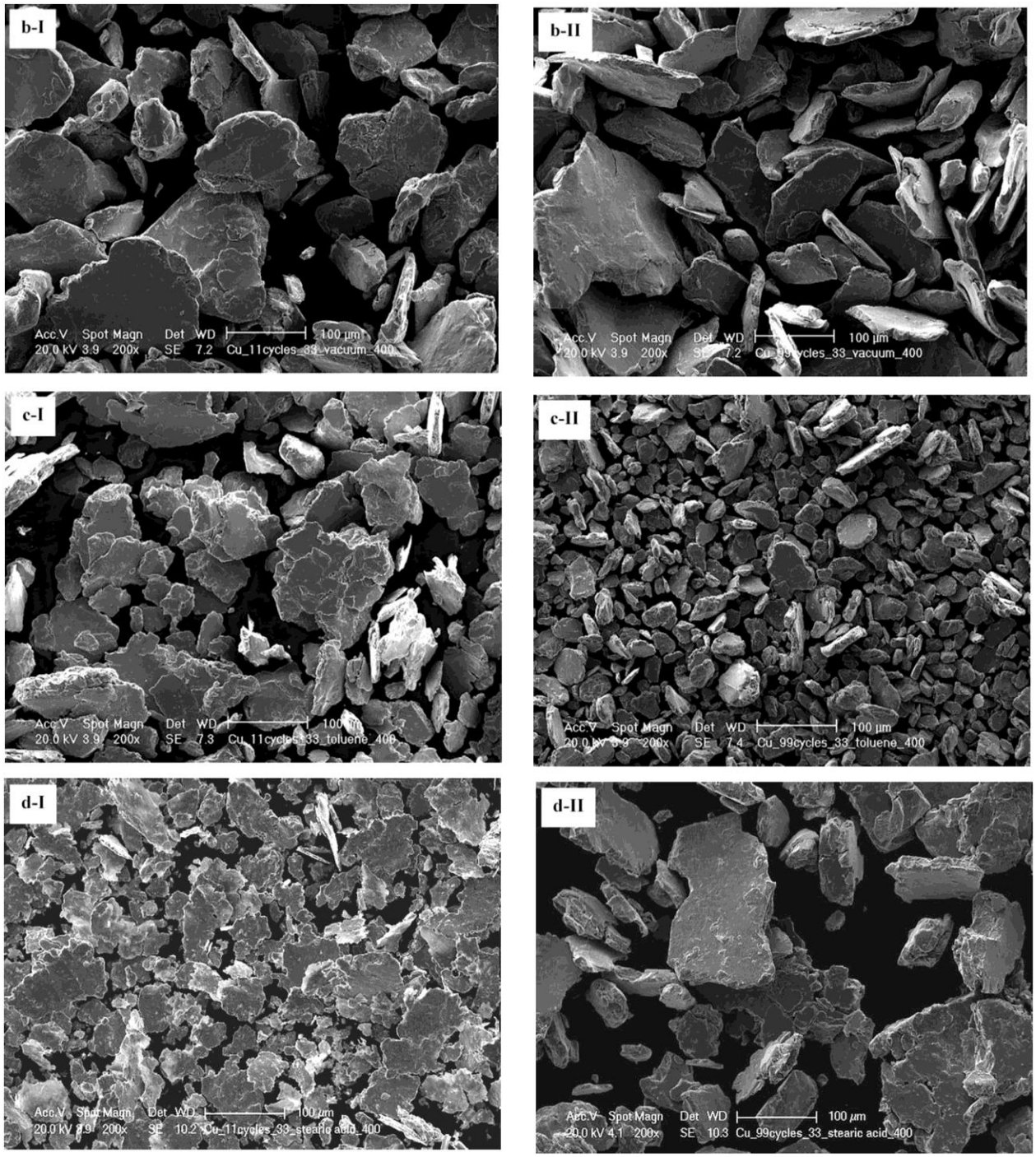

Fig 2

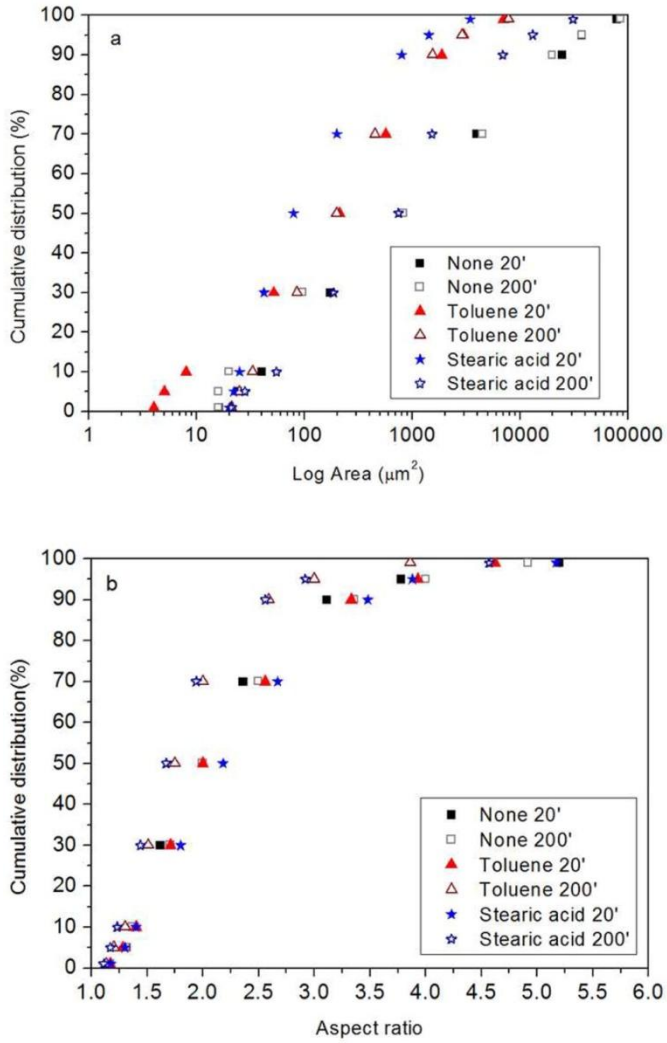

Fig 3

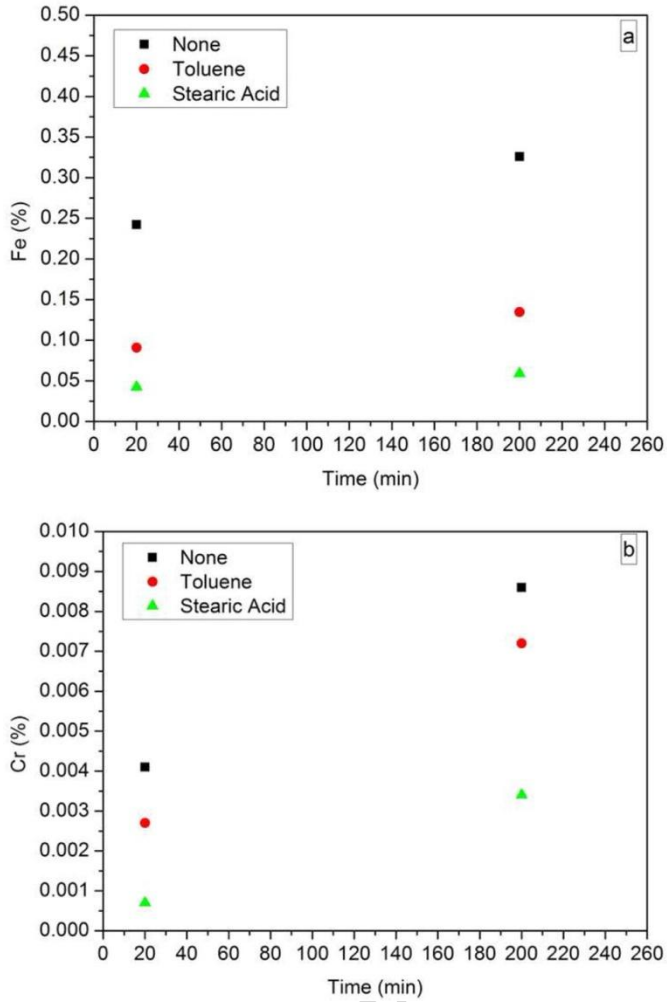

Fig 4

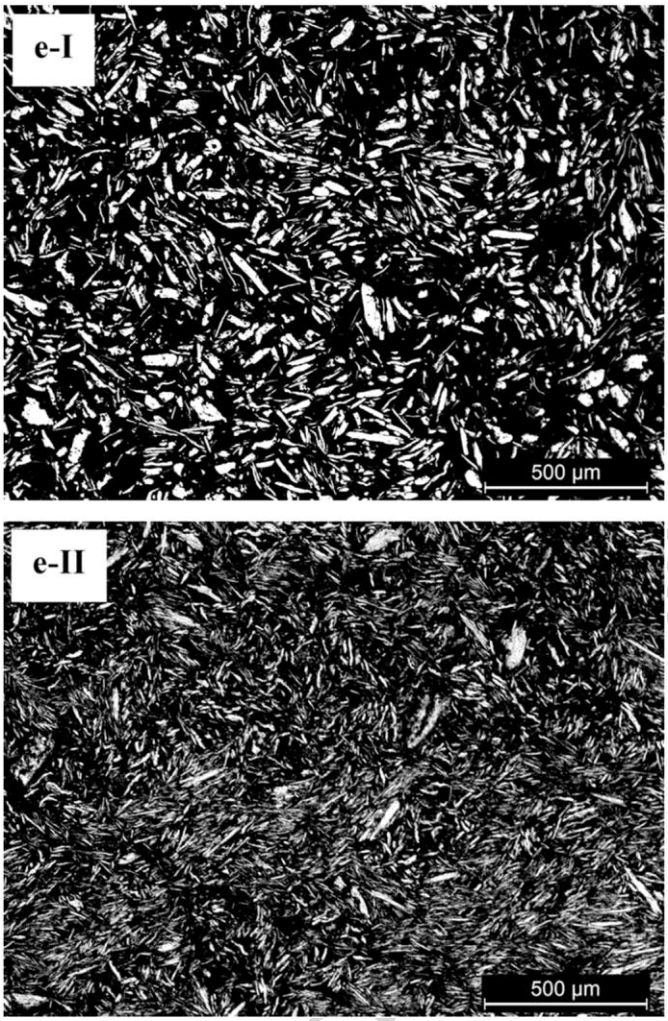

Fig 5

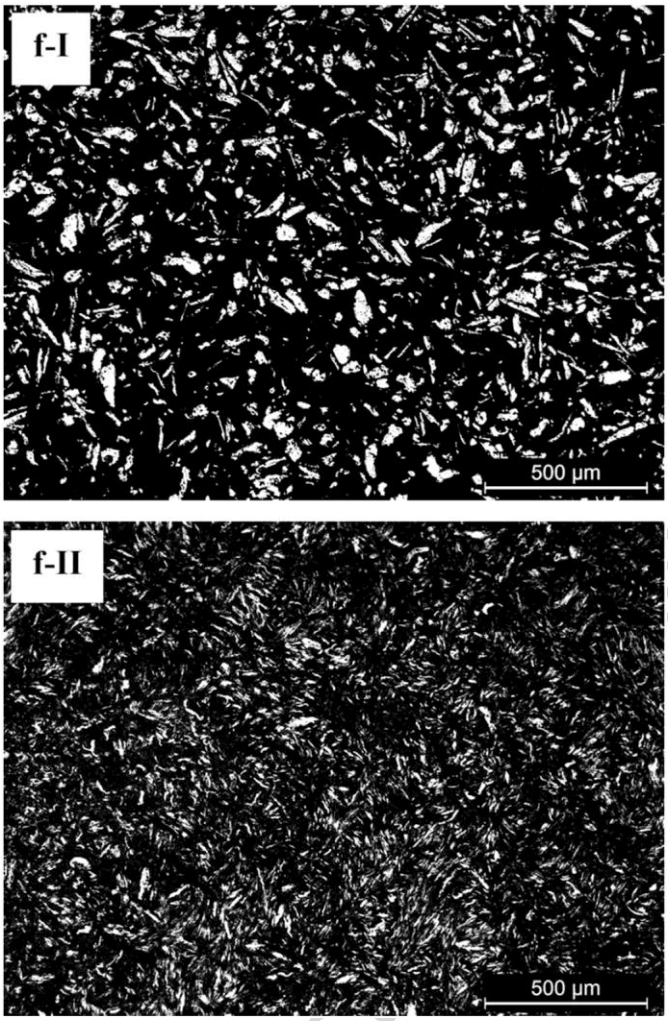

Fig 6

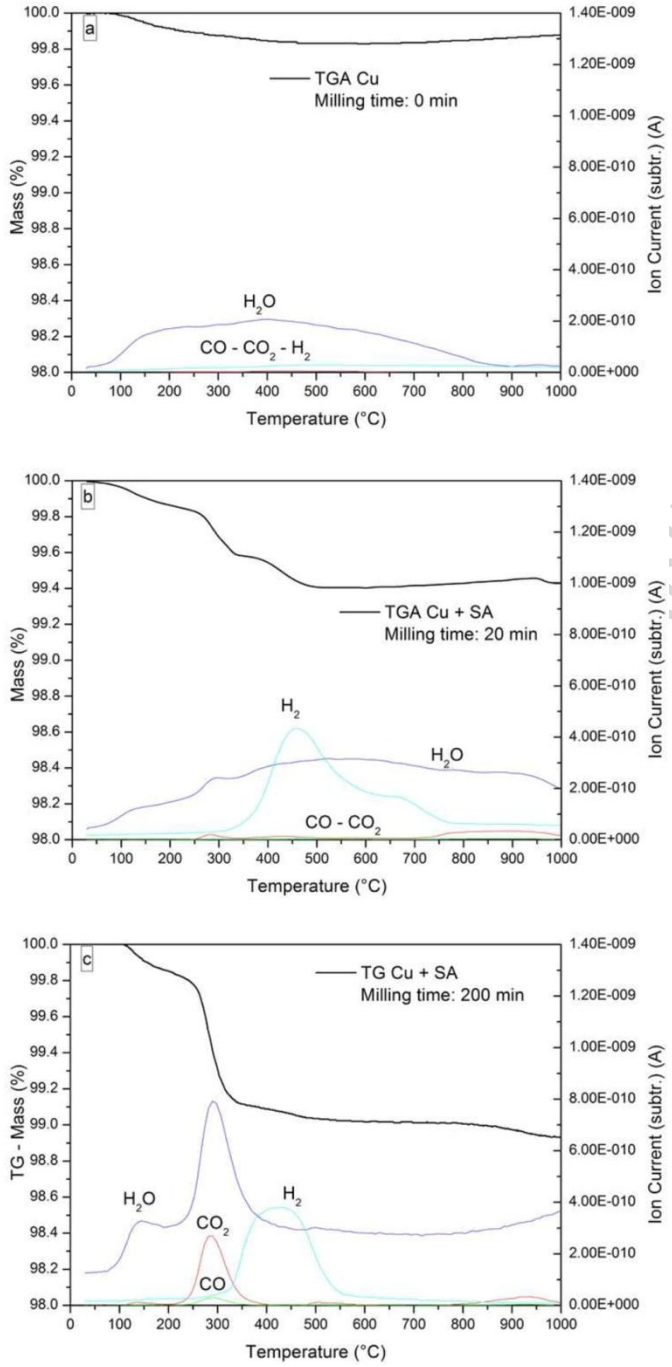

Fig 7

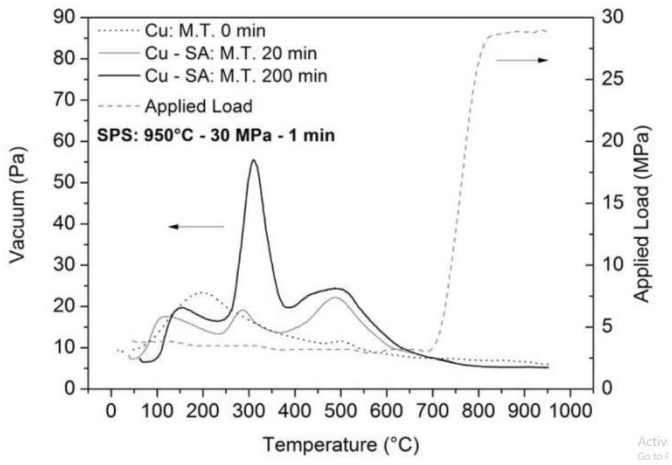

Fig 8

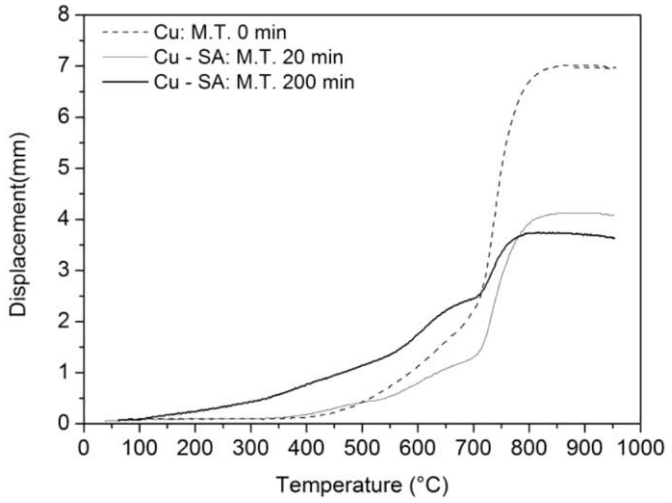

Fig 9

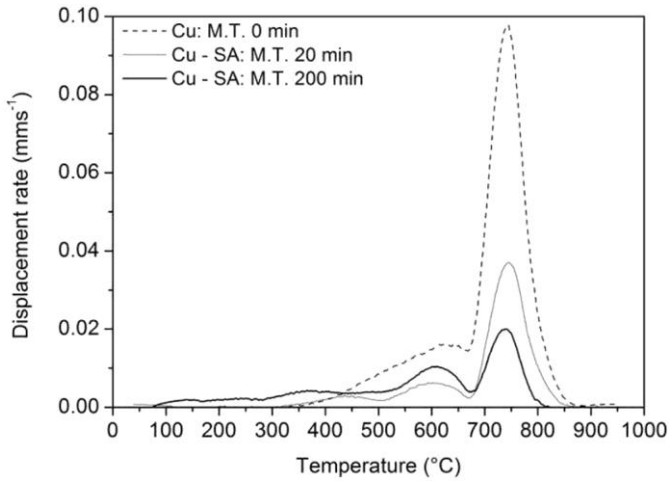

Fig 10

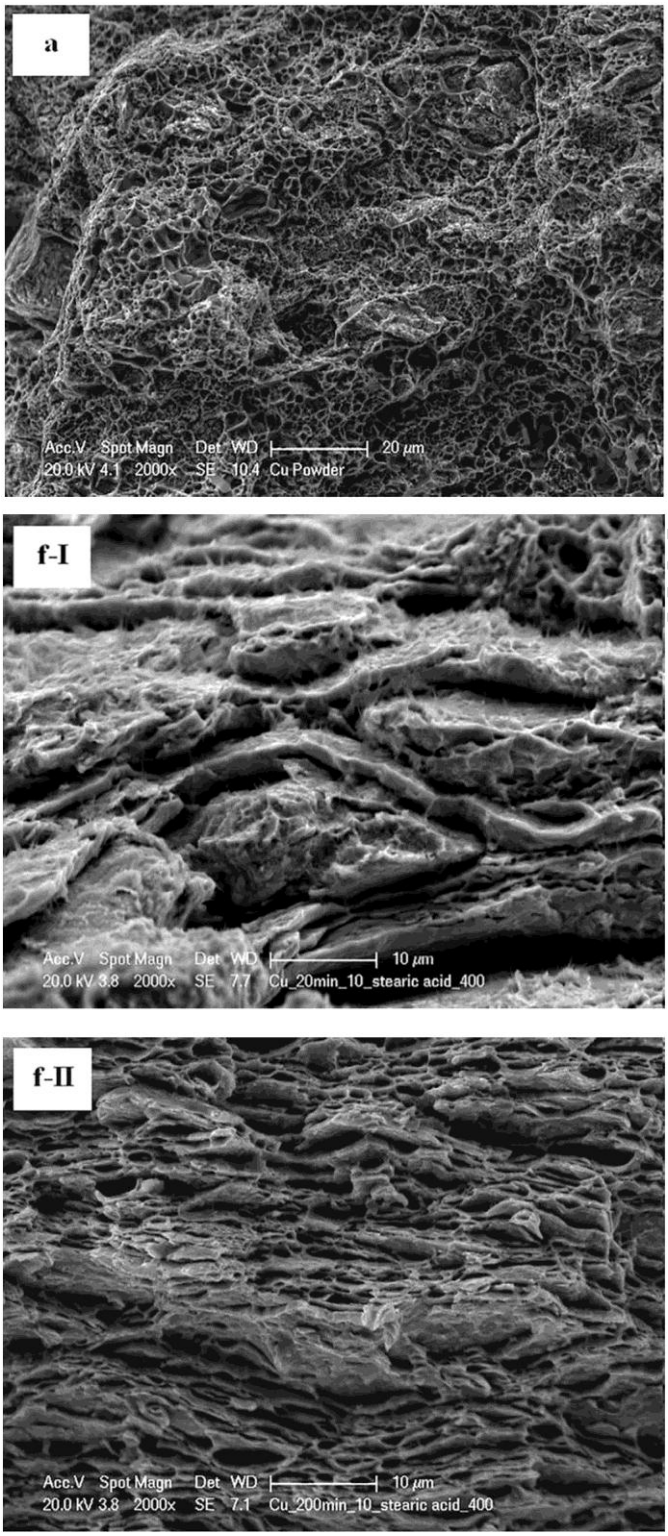

Fig 11

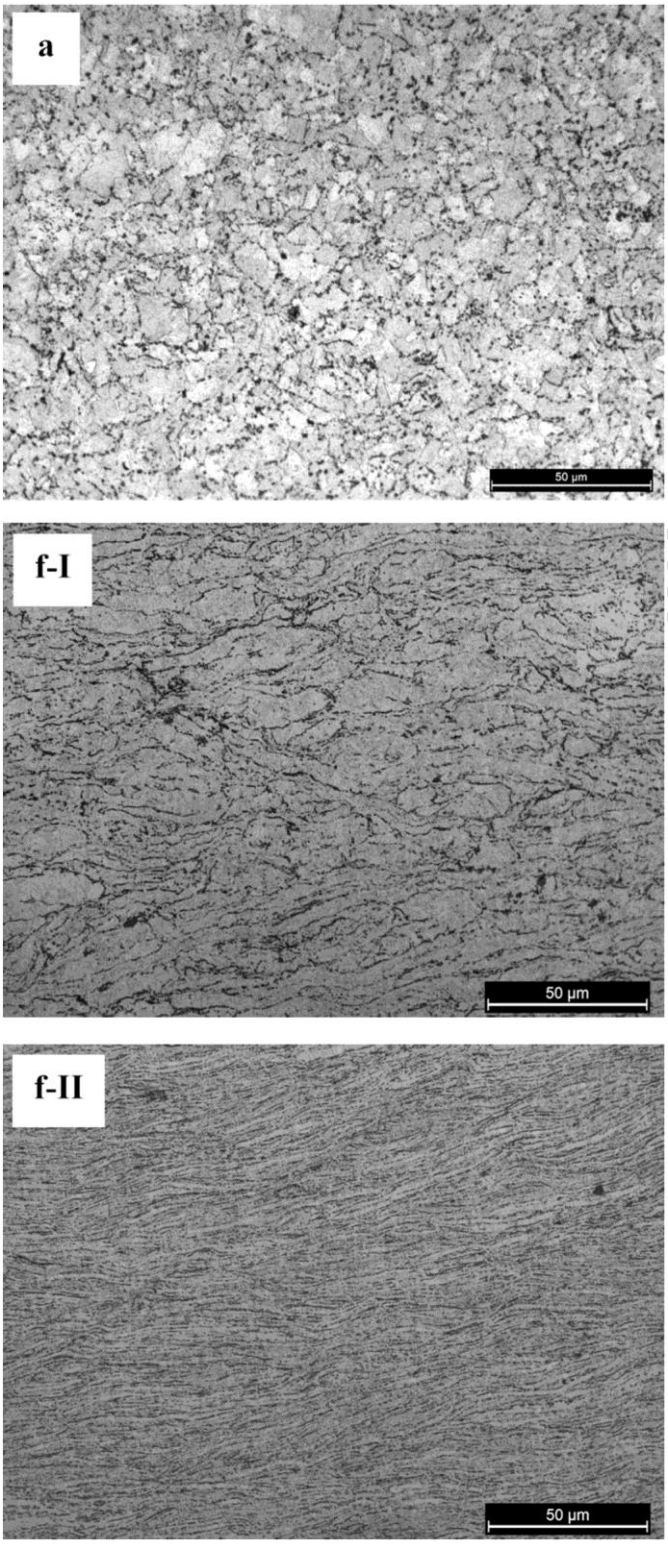

Fig 12

Step	Sample	PCA	BPR	Effective Time	Cycle
1	b-I	-	33	20	Interrupted
	b-II	-	33	200	Interrupted
	c-I	Toluene	33	20	Interrupted
	c-II	Toluene	33	200	Interrupted
	d-I	Stearic acid	33	20	Interrupted
	d-II	Stearic acid	33	200	Interrupted
2	e-I	Stearic acid	10	20	Interrupted
	e-II	Stearic acid	10	200	Interrupted
3	f-I	Stearic acid	10	20	Continuous
	f-II	Stearic acid	10	200	Continuous

Table 1: Different milling parameters

Fe contamination (%)			
Milling Time (min)	BPR 33:1 Interrupted	BPR 10:1 Interrupted	BPR 10:1 Continuous
20	0.04	0.01	0.01
200	0.06	0.01	0.01

Table 2: Fe contamination as function of ball to powder ratio (BPR) and type of cycle

LECO Analysis		
Sample	Powder	
	O (%)	C (%)
Cu	0.14	0.01
Cu + 0.5wt% S.A: milling time 20 min	0.49	0.36
Cu + 0.5wt% S.A: milling time 200 min	0.84	0.34

Table 3: Oxygen and Carbon contaminations in atomized and milled copper powders

LECO Analysis		
Sample	SPS	
	O (%)	C (%)
Cu	0.02	0.01
Cu + 0.5wt% S.A: milling time 20 min	0.21	0.06
Cu + 0.5wt% S.A: milling time 200 min	0.37	0.14

Table 4: Oxygen and Carbon contaminations after sintering

Sample	Relative density (%)	HV 0.05 Perpendicular	HV 0.05 Parallel
Cu	99	94	110
Cu + 0.5wt%S.A.:milling time 20 min	99	105	124
Cu + 0.5wt%S.A.:milling time 200 min	99	124	137

Table 5: Relative density and hardness measurements

Graphical abstract

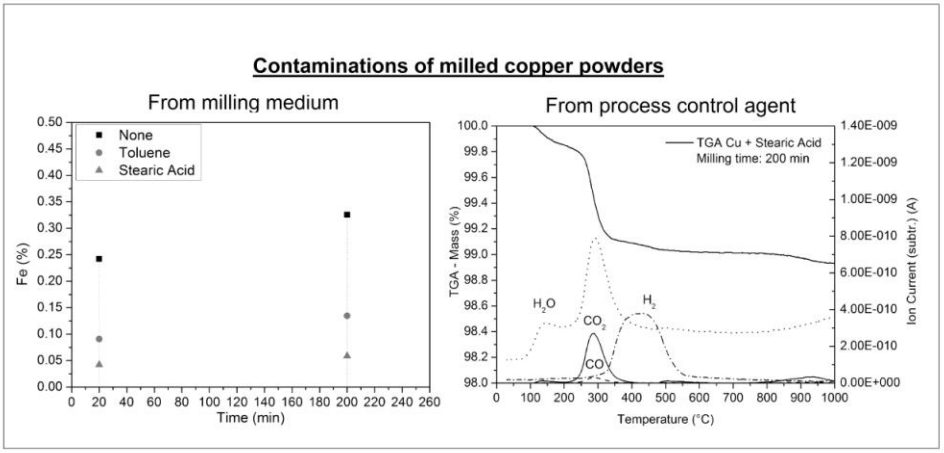

Highlights

The use of stearic acid as surfactant limits the milling medium contaminations

Decomposition of residual stearic acid occurs by the emission of H_2O, CO_2, CO and H_2

Reliability of vacuum level of SPS as a measurement of gases emission is proved

Residual porosity is properly avoid by an optimized sintering cycle